Optics & Laser Technology 181 (2025) 111592

Contents lists available at ScienceDirect

Optics and Laser Technology

journal homepage: www.elsevier.com/locate/optlastec

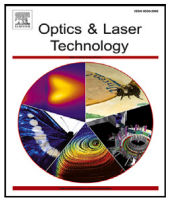

Full length article

Evaluating edge joint preparation impact on penetration depth in laser-arc hybrid welding

A. Artero-Real [a,*], M. Kristiansen [b], J. Frostevarg [c], J. Justo [a], J. Cañas [a]

[a] Escuela Técnica Superior de Ingeniería, Universidad de Sevilla, Camino de los Descubrimientos s/n, Sevilla 41092, Spain
[b] Department of Materials and Production, Aalborg University, Fibigerstraede 16, Aalborg 9220, Denmark
[c] Department of Engineering Sciences and Mathematics, Luleå, University of Technology, 971 87, Luleå, Sweden

ARTICLE INFO

Keywords:
Hybrid welding
Laser-MIG/MAG
Edge joint preparation
Surface roughness
Gap
Air volume gap

ABSTRACT

Nowadays, conventional welding technologies such as submerged arc welding (SAW) are still used in most heavy-steel industries. This type of traditional technology means that welding takes up a large part of the productive time. As a solution to this problem, there are welding methods, such as Laser-Arc Hybrid Welding (LAHW), that have the potential to reduce the cost of manufacturing large steel structures. This is possible due to the reduced number of weld passes required to join thicker steel sections, as large thicknesses can be welded in one or a few passes.

A problem with LAHW is achieving satisfactory quality. For this reason, it is essential to study the starting conditions, e.g. edge joint preparation. The target of this research work is to find out the relationship between the penetration value of the weld bead obtained and the edge joint preparation. The evolution of the molten pool and the behavior of the molten material in the joint is discussed for the different edge joint preparation configurations. The effect of the roughness is that it affects the wetting of the molten material in the joint, which would affect the penetration result, together with the gap and air volume gap used in the joint. Cut-wire is also used in the research, in samples that presented a larger air volume gap. The behavior of the molten metal inside the joint in this case is also discussed. In addition, the quality of the weld beads has also been determined by making macrographs, microstructural analysis, X-ray, microhardness profiles, tensile test and Charpy test. Some pores and cracks have been found, although destructive tests show adequate behavior of the weld bead. It is possible to elucidate from the findings that as the roughness, gap and/or air volume gap of the edge joint increases, the penetration value obtained increases. Cut-wire samples obtained full penetration.

1. Introduction

Today's metal industry of large structures is conservative and continue using conventional joining technologies, such as submerged arc welding (SAW) or semi-automatic MIG/MAG (Metal Inert/Active Gas) welding. The operation of this type of technology is well known, although it can present a problem related to working time and therefore to the productivity of this industry. For example, in the manufacturing of wind power, wind turbine towers are constructed as tubular steel towers and the welding task can consume 50% of the total production time. Self-supporting, solid wall tubular steel towers are now used for most wind turbines. The tubular steel structure is made from steel plates of a certain thickness. They are first bent and then longitudinally welded. These already bent and welded plates, known as ''cans'', are then joined by circumferential welding to form the various sections of the tower, which require a series of internal welds and surface treatments to complete them. The dimensions of these towers continue to increase with larger turbines and offshore locations in deeper water. This affects the thickness of steel used which results in several more welding passes required to complete the weld joint. An idea that can solve this productivity problem is to reduce the number of passes. One promising approach to reducing production costs for such large steel structures is the use of laser-arc hybrid welding (LAHW). According to Webster et al. [1], LAHW represents an attractive solution for joining various metallic materials and thicknesses and provides much higher penetration depths. Plates of 15–20 mm thick can be joined in one pass without beveling. According to Nielsen [2], due to the high energy density of lasers in LAHW, this eliminates the number of passes and minimizes heat distortion as compared to conventional arc welding techniques, resulting in reduced heat loss due to high intensity. A recent study by Bunaziv et al. [3] concluded that LAHW is more productive than GMAW due to its high penetration depth,

* Corresponding author.
E-mail address: aartero@us.es (A. Artero-Real).

https://doi.org/10.1016/j.optlastec.2024.111592
Received 19 April 2024; Received in revised form 18 July 2024; Accepted 6 August 2024
Available online 20 August 2024

requiring significantly fewer passes. Additionally, LAHW consumes half the energy of GMAW. The use of welding consumables for LAHW is significantly lower because LAHW requires much less beveling.

Although this technology shows great potential, it is important to emphasize that laser-arc hybrid welding has a high tendency to form pores in the root as the thickness of the plate to be welded increases. In addition to other well-known problems such as concavity, undercut, root humping or cracks [4]. The groove width and area of the hybrid weld could be reduced by about 45% and 65% compared to the MAG weld, because laser-arc hybrid welding requires much less deposited metal and power used during welding [5]. With hybrid welding, the productivity of the final product increases and the production cost is reduced [5], moreover this welding method can provide higher impact toughness than conventional welding methods [6]. This is a very important feature in welded structures. According to the results of Kannan et al. [7], the number of passes influenced the final microstructure. In their study, they compared a weld bead made with one pass of LAHW to one made with two passes of LAHW. The weld bead with two passes has a higher amount of acicular ferrite in the fusion zone than the weld bead with one pass. This is due to the filler material, as in the case of two-pass welding, more of the wire is fed from the electric arc. As a result of the chemical components of the filler wire, more acicular ferrite will be generated.

Sokolov et al. [8] concluded that, at high power levels, absorption has a significant dependence on the edge surface roughness in thick section laser beam welding. The efficiency of laser beam welding can be improved by increasing the absorption through the laser energy consumed by the keyhole walls. Later in [9], Sokolov et al. worked with 20 mm thick S355 steel in I-butt joint configuration and concluded that in order to achieve higher productivity of laser beam welding, the joint should be prepared with an abrasive water jet cut. Another very important starting point for this research is the work of Farrokhi et al. [10], in which, among other conclusions, they saw that using plates with laser-cut edges and no preset gaps, the welding travel speed can be increased by up to 130%. Furthermore, they checked that turbulent vertical striation caused by laser cutting could lead to higher welding travel speed compared to the systematic square-shaped pattern caused by milling tools.

To achieve a good welding result, the surface tension of the molten metal at the root must withstand and balance the downward melt flows due to dynamic recoil pressure and gravitational force caused by the mass of the melt column above the root [11]. Thus, a backing method is considered to be used to support the molten metal of thick plate joints with relatively wide gaps. However, the welding process would fail if the laser beam interacts with the backing material. So, the backing needs to be protected from laser radiation by filling the air gap in the groove with a material filler. In this way, Wahba et al. [11] filled with cut-wire particles, that is fine pieces of the same composition as the MAG filler wire, cut to a length similar to the diameter. In the present work this idea is reproduced. Other authors such as Bunaziv et al. [12] discovered that insufficient filler wire can be supplied in the root with standard LAHW and this is associated with numerous technical problems because it directly affects the mechanical properties. One of the positive effects of adding the cut-wire to the joint is that the hardness obtained from vertical hardness measurements showed that the transition between the arc zone and the laser zone was much smoother than when no cut-wire was added. As the final result of the weld bead is more homogeneous than if it is not added.

According to Bunaziv et al. [13], LAHW is susceptible to root humping due to unfavorable melt flow at the bottom of the weld pool so that wide fusion zone width in the root causes dropouts and sagging. Authors such as Silva et al. [14], comment on the differences between different types of backing, concluding that there are several commonly employed backing materials, such as ceramic, copper and fiberglass, each with its own advantages and limitations. The copper backing is characterized by its remarkable thermal conductivity, which aids in the solidification process and provides mechanical support to the weld root. On the other hand, fiberglass backing offers flexibility, ease of application and the key advantage of allowing gas flow to some extent within the bevel. Finally, ceramic backing can present a challenge due to its high melting point, which makes it difficult to fuse with the weld, although the thermal conductivity is really low, which means they can withstand high temperatures without transmitting heat to the rest of the environment. This can help concentrate the heat from the welding process at the root of the weld bead. Other authors such as Uemura et al. [15], use a backing sheet for welding vertically up. In this way, they avoided the dripping of the molten pool, obtaining stability in the weld bead. Üstündağ et al. [16] tried to solve the problem of single pass welding in flat position with gravity dropout at low welding velocities using an electromagnetic weld pool support system. In [17], they achieved gap bridgeability up to 1 mm by welding of 20 mm thick plates in flat position.

Üstündağ et al. [18] showed their edge preparation for laser and plasma cut samples. The cut edges exhibit characteristic features. Laser-cut samples displayed striations that are clearly defined at the top of the cut edge and become coarse towards the bottom. However, in their research, the focus was not primarily on the cutting experiments, but rather on investigating the impact of edge quality on the weld bead quality during single-pass LAHW with electromagnetic weld pool support instead of ceramic backing. Bunaziv et al. [13], work with thicknesses of 12 to 15 mm plates of thermomechanically rolled structural steel. These authors studied 2 types of preparations, machined and plasma cut surfaces, and also measured their roughness. They concluded that the process window for the specimens with the machined joint was larger than for those prepared by plasma cutting. Previously, authors such as Sokolov et al. [8], that worked in laser welding, studied the influence of surface roughness and weld bead penetration. and they concluded that the highest penetration depth at power levels of 14 and 10 kW was achieved at $R_a = 6.3$ µm. Following the path of the above-mentioned investigations, the main idea of this research is to link the surface roughness knowledge with LAHW welding, as well as to Üstündağ et al. [18], which works with thicknesses of 20 mm of laser and plasma cutting samples. For this research has been decided to work in a single pass with 20 mm thick plates because it was expected that with the parameters that was being used, the full thickness could be achieved, or at least be close to it. In this way, it was possible to study how the roughness of the joint edges influences the final penetration of the weld bead. Furthermore, the research tries to find an answer to the penetration performance when the roughness of the weld joint changes.

2. Methodology

The main objective of this research is to find out the relationship between LAHW weld bead penetration and edge joints preparation of thick steel plates in a single pass in an I-butt joint configuration. The different edge joints preparation are 3 machined surfaces, plasma cutting and abrasive water jet cutting. One of the parameters chosen to know the quality of the weld bead is the penetration achieved. In this way, it will be discussed whether it is beneficial to the industry to use the surface of the joint without conventional machining. Therefore, the differences in the penetration results of the different weld beads will be shown. Fig. 1 shows the study structure of this research, which is similar to that of previous work by Farrokhi et al. [19]. This study structure is fully related to the sections of this research. Section 2.1 is the cutting procedure, which explains how the different surfaces used in the research were obtained. Then, the quality of the surfaces is measured and it is explained in Section 3.1. Once the roughness has been measured, Section 2.2 shows the welding set-up and the parameters used, and Section 2.3 shows the testing equipment used. Finally, in Section 3.2, the results obtained for the weld beads through visual inspection, X-ray, macrographs, microstructure study, tensile test, Charpy test and microhardness profiles are shown.

Table 1
Chemical composition of the base and filler materials (%). Notes: CEV according to IIW. Balance: iron (Fe).

	C	Mn	P	S	Si	Cu	Al	Ni	Cr	V	Nb	Mo	Ti	N	CEV
S355J2	0.15	1.45	0.01	0.006	0.20	0.02	0.036	0.02	0.06	0.004	0.03	0.002	0.001	0.007	0.41
Filler wire	0.07	1.43	0.011	0.014	0.87	0.08	0.001	0.01	0.02	<0.01	–	<0.01	0.01 (+Zr)	–	0.32

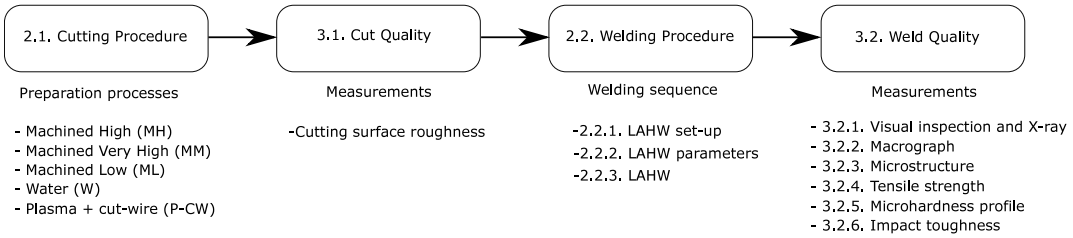

Fig. 1. Structure of the study presented in this paper.

The base material used in this research is S355J2, where slices of 21 mm × 120 mm × 120 mm were cut from a steel bar. Then, they were milled to obtain 20 mm of final thickness, and after this, the joints were prepared by modifying one edge of the slices with different preparation methods. After that, the roughness of the different surfaces was measured. Once the slices were obtained and the different surface types measured, tack welding was carried out to build the samples. Finally, hybrid welding were performed. For this task, the filler wire used was ESAB OK AristoRod 12.50 with a diameter of 1.2 mm. The chemical composition of the base and the filler wire materials are presented in Table 1.

2.1. Cutting procedure

In order to investigate the impact of different edge surface characteristics on the subsequent efficiency of the welding process, various edge surfaces were investigated. 3 cutting methods were carried out: plasma cutting, abrasive water cutting and machining with 3 different levels of roughness. Therefore, the following types of preparations can be differentiated: plasma cutting (P) + cut-wire (CW) added inside the joint, P-CW; water abrasive cutting, W; machined with high roughness, MH; machined with low roughness, ML and machined with wavy edge, MM. See Fig. 2 with an example of the different edges obtained.

The machine used for the MH and ML machined samples operated at 2100 mm/min for feed rate and 400 rpm for spindle speed in the case of MH, while for ML, it ran at 700 mm/min and 500 rpm respectively. The machine used for machined samples MM works with a tool rotation speed of 1250 rpm, a tool inclination angle of 45° and a travel speed of 2000 mm/min. Plasma cut process parameters for P-CW samples were 1000 mm/min of travel speed, using O_2 as gas type with 10 bar gas pressure, 5 mm nozzle standoff, 148 V voltage and 200 A current. Water cut process parameters for W samples (abrasive type: GMA Garnet 80) were 30 mm/min of travel speed and 15 mm/min at the start/end, 2 mm nozzle standoff, 0.76 mm nozzle diameter and 3100 bar water pressure. In the preparation of the weld joints, these were not cleaned with sandblasting or any other type of steel cleaning method. The edges were intentionally left intact from the cutting process.

2.2. Welding procedure

2.2.1. Laser-arc hybrid welding set-up

The experiments shown in this research lasted for one year, during which time the laboratory underwent modifications in its set-up. As a consequence, two experimental set-ups were used for this study. The first set-up is characterized by having, for hybrid welding, a Trumpf TruDisk 16002 16 kW continuous wave disk laser with a wavelength of 1030 nm and 200 μm fiber. Optical fiber to a Trumpf RFO Reflecting Focus Optics. The arc welding machine is a Fronius Trans Plus Synergic

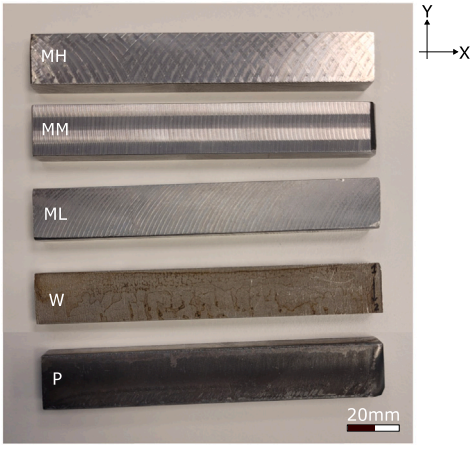

Fig. 2. Types of edges preparations: MH, MM, ML, W and P.

5000 CMT (Cold Metal Transfer) and the manipulator is a Fanuc Robot M-710i C170 and 82%Ar-18%CO_2 as shielding gas. In the case of the second set-up, a 600 μm fiber was used, the robot is a KUKA KR 30 HA, optical fiber to a TRUMPF CFO Focus Optics and arc welding machine is a Fronius 400I CMT. Fig. 3 shows both set-ups for the welding task, where it is possible to see the robotic arm that holds the arc welding torch together with the laser head and the sample placed on the work table ready to be welded.

2.2.2. Laser-arc hybrid welding parameters

In Table 2 the parameters for LAHW welding are shown. In the case of the first set-up (first welding stage), a range is displayed showing the maximum and minimum values used, since many tests with different variations were carried out. In the second set-up the parameters were completely set to those shown in the table. In set-up 2, the maximum laser power was 13 kW. Due to laboratory limitations, this was the maximum setting. It was also an adequate value obtained from the experience of the first welding stage.

An important issue is the power output parameter, as it will be mentioned continuously throughout the paper. It is the energy leaving the welding head to the sample. Heat input cannot be fully measured, it depends a lot on the energy actually absorbed in the material during process. To calculate the power output per pass (kJ/mm), the power of laser, P_L will be added to the power of arc, P_A; obtained as the product of the average value of the voltage and current. Finally, this is divided by the welding speed, v. In addition, the efficiency of both sources needs to be taken into account, η_L is the efficiency of the laser,

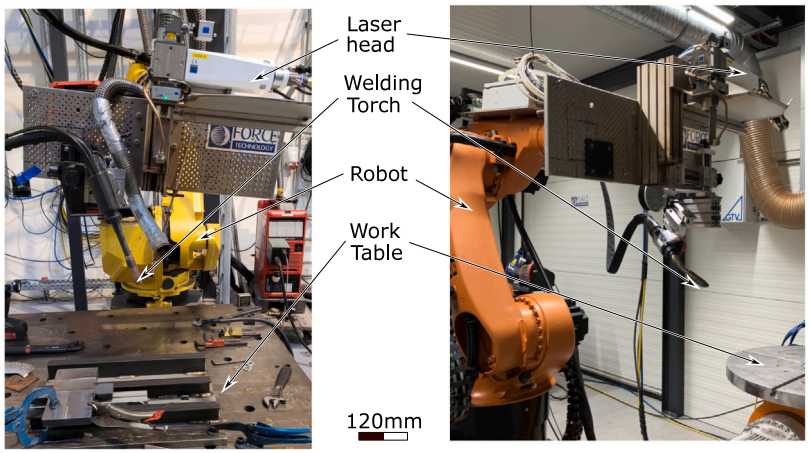

Fig. 3. First (left) and second (right) LAHW welding set-ups used in the research.

Table 2
Welding process parameters.

	Laser length fiber (μm)	Laser power (kW)	Arc power (kW)	Wire feed (m/min)	Travel speed (m/min)	Gas flow rate (l/min)	Focal position (mm)	Focal length (mm)	Laser angle (degree)	Arc torch angle (degree)	Wire stick-out (mm)	Arc-laser distance (mm)	Arc type[a]	Arc correction (%)
Set-up 1	200	[10,16]	[2.7,18.2]	[8,20]	[0.5,1.2]	20,25	[−10,50]	600	−7	20	20,25	[2,15]	S, P, CMT+P	[0,15]
Set-up 2	600	13	6.49	10	0.8	20	10	600	−7	20	17	2	CMT+P	0

[a] (Arc type: Standard (S), Pulsed (P) and Cold Metal Transfer (CMT)).

and η_A the efficiency of the arc.

$$P_{out}\ [\mathrm{kJ/mm}] = \frac{P_L\ [\mathrm{kW}] \cdot \eta_L + (V \cdot I)\ [\mathrm{kW}] \cdot \eta_A}{v\ [\mathrm{mm/s}]}$$

The CMTP mode is always used in the second welding stage, which results in the graph shown in Section 3.3. Authors like Bunaziv et al. [20,21] also use CMT+P as arc mode and, according to them, the application of CMT + P arc has high potential in the industry because it is possible to reduce the power output and the grain growth in the coarse grain heated affected zone (CGHAZ).

2.2.3. Laser-arc hybrid welding

Regarding the LAHW welding process, it is possible to see in Fig. 4 the prepared welding sample with four tack welds. The gap is prefixed to avoid movements of the parts during welding and also to discard the beginning and end of the weld bead. In such a way that it is only necessary to place the sample on the work table and set the robot path to follow, making the welding set-up fast and robust, since the welding task can be carried out in less time. This figure also shows a schematic preview of the full experimental procedure.

It was decided to use a ceramic backing in the tests carried out in the present investigation, placed on the lower part of the weld bead using aluminum adhesive tape. As it was previously said, the gap is fixed with tack welding, for water and plasma cut methods was used 0.3 mm of gap, and for machined samples 0.5 mm. In both cases with a tolerance of ±0.15 mm. Another important aspect of the chosen configuration is the process that leads the movement. In this case, laser leading has been chosen. Some authors, such as Bunaziv et al. [20], concluded that the arrangement of the torch has influence on process stability. In their conclusions, it was mentioned that when a leading arc configuration is used, the droplet flight can affect the keyhole opening, resulting in pores in the weld.

2.3. Testing equipment and weld inspections

The inspection of cut quality was carried out using an optical microscope Zeiss Axio Imager 2, equipped with an automatic image-stitching program. After welding, the quality of the weld bead was studied and the first steps were X-ray inspection with the objective of detecting possible porosity and cracks in the welds. However, prior to this X-ray inspection, a visual inspection of the weld beads was performed: top, bottom and cross section view. For this purpose, an image was taken of each view of each sample.

The same microscope used previously for the roughness measurement was also used to obtain the macrographs and microstructure. As a preliminary step for the macrographs, a sample of the weld bead had to be cut, sanded and polished. Finally, the microstructure was revealed by dipping the fully polished sample in 2% Nital for 10 s. Once the macrographs had been obtained and the microstructure studied, the same samples were used to obtain the microhardness profiles. Macrographic samples were tested for Vickers hardness with a Struers Duramin 40 hardness tester (HV1). For each sample, the microhardness profile in the arc zone and in the laser zone was studied. For each zone, a straight pattern with 50 measurements was drawn.

The machine used for the tensile test was an Instron 5568 universal testing machine. In order to study the tensile properties of joints welded with S355J2 using different welding parameters, tensile tests were carried out on two specimens: one from the arc zone and one from the laser zone. Fig. 5 shows the size of the tensile test samples, as well as where they were obtained. From each weld sample, both samples were obtained according to the ISO 4136: 2012 standard, with a thickness of 2 mm.

The Charpy pendulum machine was a LOSENHAUSEN Impact Tester PSW30. The Charpy tests were performed at room temperature (20 °C) due to the laboratory's available resources. Authors such as Bunaziv et al. [13,22] performed the notch in both fusion line (FL) and weld zone (WZ). In [13], they showed that the FL zone obtained lower toughness values than in the WZ. Based on these results, it was decided to perform the notch in the FL, where it is straight and perpendicular to the plate thickness direction, as it could be more critical. The dimensions of the sample are 55 × 10 × 10 mm according to ISO 148-1:2016 standard (see Fig. 5).

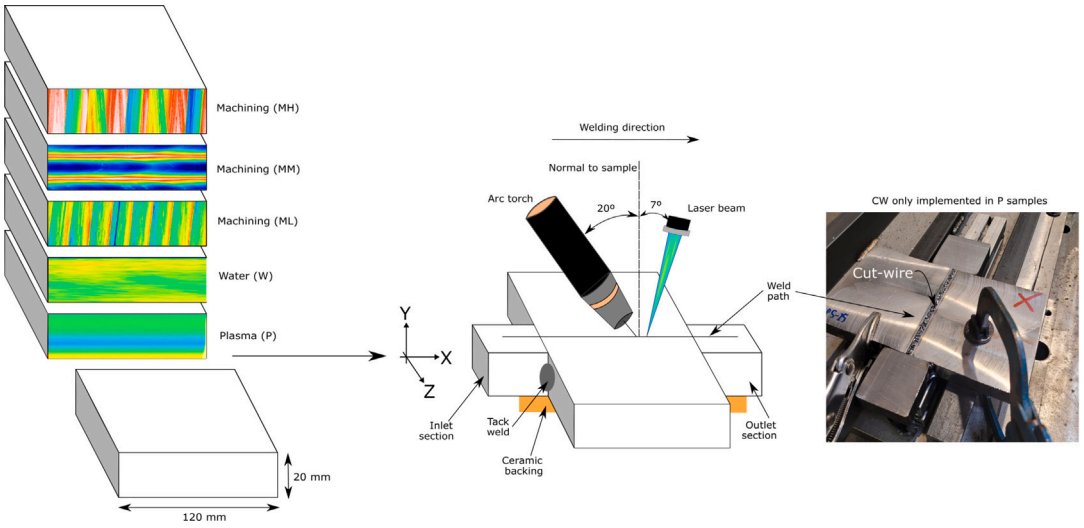

Fig. 4. Schematic view of the experimental procedure and sample filled with cut-wire.

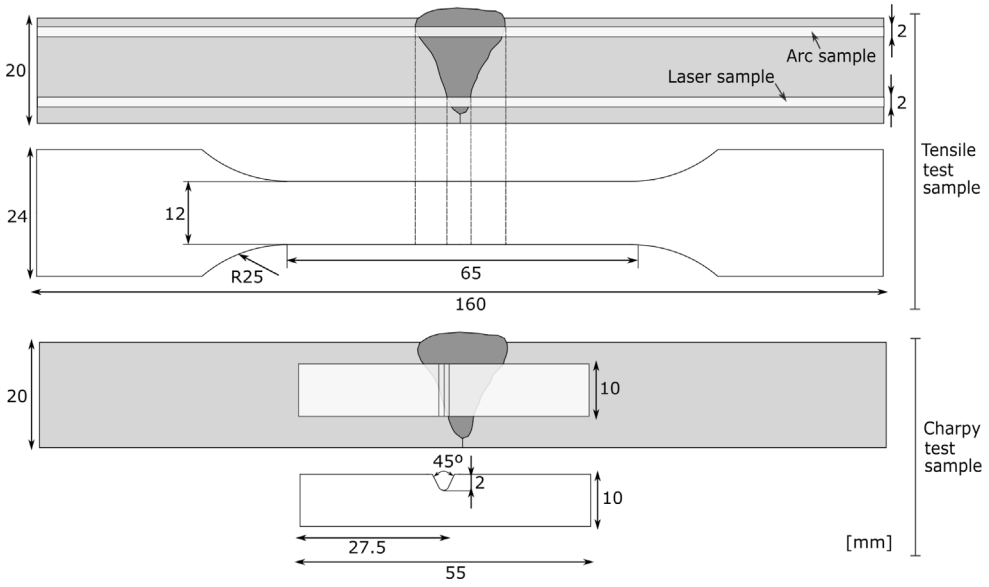

Fig. 5. Dimensions of tensile and Charpy test specimens.

3. Results and discussion

In this section, first, the quality of the cut preparation is quantified. Then the quality of the weld through destructive and non-destructive tests is studied. The main purpose is to relate how the cut preparation influences the weld quality.

3.1. Cut quality

Topographic maps were made in the 'X' and 'Y' directions. For the case of machining, one measure in 'X' and one in 'Y', for the case of plasma, since it had a burr at the end of the cut, two measurements in 'X' and one in 'Y' were made, and finally for the surface cut with water, three measurements were made in 'X' and one in 'Y'. Fig. 6 shows the topographic surfaces in 'Y' direction (along the thickness of the sample) made with the microscope. Once the topographic map has been made, a specific profile can be extracted from it to determine the roughness parameters. This information was extracted from the reports generated by the microscope AxioVisio program. Here it is possible to see not only the roughness profile, but also the size of the edge. It can be easily seen that the plasma sample has a very large burr (its scale is in mm, while the rest is in μm), making direct welding unfeasible without previously performing a grinding operation. For this reason, these samples were finally used to be filled with cut-wire inside the joint. Fig. 4 shows the cut-wire configuration, which consists of the joint of the plasma cut samples filled with small pieces of filler wire. During the welding process, there was never a problem with the loss of these elements due to the shielding gas coming out of the MAG torch.

Fig. 6 shows the results of roughness, where the value of the parameter R_c is specified according to the standard ISO 4287:1997, where the mentioned parameter is the average value of the heights of the profile elements, measured on the roughness profile. A Gaussian filter equal to the 5th part of the total evaluation length was used to obtain these roughness parameters. Evaluating the roughness values of Fig. 6 it can be seen that the values measured vertically are in agreement with those measured horizontally, except for the plasma sample. In the case of the water cut sample, the values of the 3 horizontal roughness measurements are very similar, but slightly lower than the vertical roughness value. The special shape of the edge of the MM sample, due to the way it has been machined, also causes the measured value to

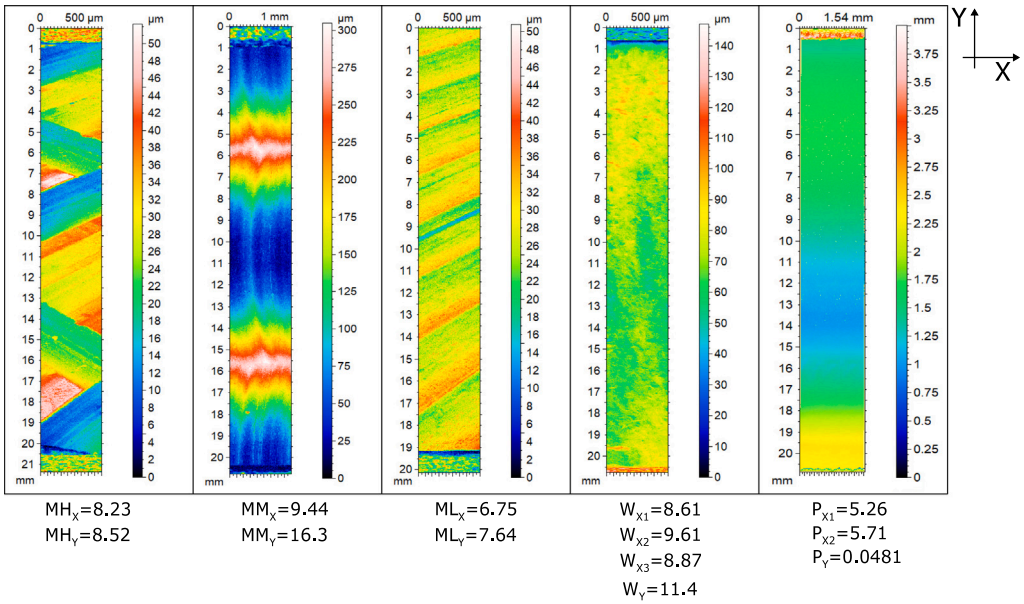

Fig. 6. Topographic maps of different surfaces MH, MM, ML, W and P (in 'Y' direction), with roughness results [R_c (μm)] according to ISO 4287:1997.

differ vertically and horizontally, making it exhibit the highest value of vertical roughness.

3.2. Weld quality

From the first welding stage, where multiple tests were performed with different parameter settings, the procedure for obtaining results was as follows: A visual inspection was carried out, followed by radiography of the samples that performed best in terms of penetration and quality of the top of the bead. The next step was to choose those samples that had some special characteristic (for example, ML1 is characterized by the fact that it was only laser welded and MM6 for being the only sample with two passes) or good quality, to perform macrographs, microstructure study, microhardness profiles, tensile test and Charpy test. In these last three tests, a differentiation is made between the arc zone and the laser zone. In the second stage, only a few macrographs and microhardness profiles were obtained, one for each type of roughness, after the samples had been examined visually. Due to resource limitations in the laboratory, it was not possible to perform a larger number of tensile and Charpy test specimens for each weld bead.

Table 3 shows the power output used for welding and the results obtained for different specimens (from the first welding stage), which will be discussed from Sections 3.2.1 to 3.2.6. The values are ordered from the smallest (0.86 kJ/mm) to the largest (3.43 kJ/mm) power output. In the case of the second experimental set-up, taking into account that the welding parameters were the same, the power output also has a constant value of 1.36 kJ/mm. These values are in line with the values used by other authors such as Zhou et al. [23] performed 3 passes with a total power output between 3.5 and 4 kJ/mm, working with Q235 steel grade, as well as Zhen et al. [5], welding with 3 kJ/mm in 3 passes, but working in S355J2W+N. Bunaziv et al. [20] uses power outputs between 1.4 and 2.1 kJ working with high-strength steel plates and Üstündağ et al. [18] working with 1.9 kJ/mm and S355J2. Farrokhi et al. [24] performed a successful one-pass weld of 25 mm thickness with 2.82 kJ/mm in S355J2 steel and ceramic backing.

3.2.1. Visual inspection and X-ray

Visual inspection reveals good appearance in most of the weld beads at the top. At the bottom, lack of penetration is present in almost all samples, see Fig. 7(A)i and (C)i. Complete penetration is present in few samples, see Fig. 7(B)i. Root cavities at the weld root is shown in Fig. 7 (D)i, where the laser beam interacted with the ceramic backing. With visual inspection, it was possible to see the effect of the heat increasing with increased roughness also in the weld root.

X-rays were taken from the top of the sample ('Y' direction) to study the inside of the weld bead, looking for pores or cracks, since the visual inspection could detect the clear lack of penetration, but the quality of the internal result was unknown. For example, Fig. 7(A)ii clearly shows good weld bead quality (except for the lack of penetration) and Fig. 7(C)ii shows cracks and lack of penetration, although most of the samples show no porosity. Fig. 7(B)ii shows complete penetration and no porosity or cracks.

In order to know the final value of the penetration, different techniques were studied. The first was to use X-rays but using a side view ('Z' direction) instead of a top view ('Y' direction). With the objective of seeing the evolution of the weld root along the entire length. Previously, it was known that the lack of penetration was varying because a feeler gauge was introduced into the welded joint and it was found that the lack of penetration varied by up to 4 mm. This way of measuring penetration was discarded, since it was not accurate.

An option studied was to cut the weld bead in half and see how the penetration evolved, as can be seen in Fig. 7(E). This method was valid to know the penetration but had two clear disadvantages: it was very time consuming and it also left the specimen completely destroyed, so it was discarded. The method chosen to know the penetration depth was to machine the weld root until the full penetration was found and it was clearly observed that there was a complete fusion. Using this technique, it is still possible to use the specimen for mechanical testing.

The conventional X-ray view ('Y' direction) made in the first welding stage showed that in some water cut samples it is possible to see a solidification crack pattern in Fig. 7(C)ii. According to Hassel et al. [25], in their research, they showed how cracks are formed by solidification and divided crack formation into three different phases. During the first phase of solidification, the dendrites undergo unrestricted growth. Subsequently, in the second phase, the fusion zones on opposite sides make partial contact, giving rise to closed regions. These regions exhibit contraction stresses which exert outward pressure on the melt surfaces. Consequently, separations occur within the liquid phase in these specific regions. In the third phase, local solidification is completed. The separated zones can be filled with molten material if a suitable amount is available. However, in cases where there is not

Table 3
Power outputs with mechanical results. Note: For power output calculations, 100% laser efficiency η_L and 80% arc efficiency η_A have been assumed.

	MH1	MH8	W14	W11	MM10	W8	MM6	W19	ML1	W15	P-CW6	ML3	ML8
Power output (kJ/mm)	0.86	0.91	0.91	0.91	0.99	1.14	1.17 1.17[a]	1.18	1.44	1.44	1.66	2.04	3.43
Tensile strength arc (MPa)	515.6	521.0	505.8	521.1	512.1	–	–	518.2	–	505.9	513.9	504.5	520.4
Tensile strength laser (MPa)	516.2	X	X	X	513.9	–	511.9[b]	X	523.1[b]	508.9	X	507.4	520.5
Elongation at break arc (%)	17.14	15.01	14.48	16.86	13.97	–	–	15.26	–	14.83	12.52	6.83	7.20
Elongation at break laser (%)	20.62	X	X	X	18.27	–	7.16[b]	X	11.80[b]	16.17	X	19.32	15.63
Max micro- hardness (HV1)	428.6	411.8	411.8	–	395.9	388.2	420.2	388.4	287.3	280.9	288.8	323.1	222.0
Impact toughness (J)	155.1	156.1	141.3	–	139.4	119.7	152.1	88.3	152.6	147.7	155.1	175.2	70.7

[a] Two pass double side welding.
[b] Not broken at all, stopped in necking (outside the weld bead).

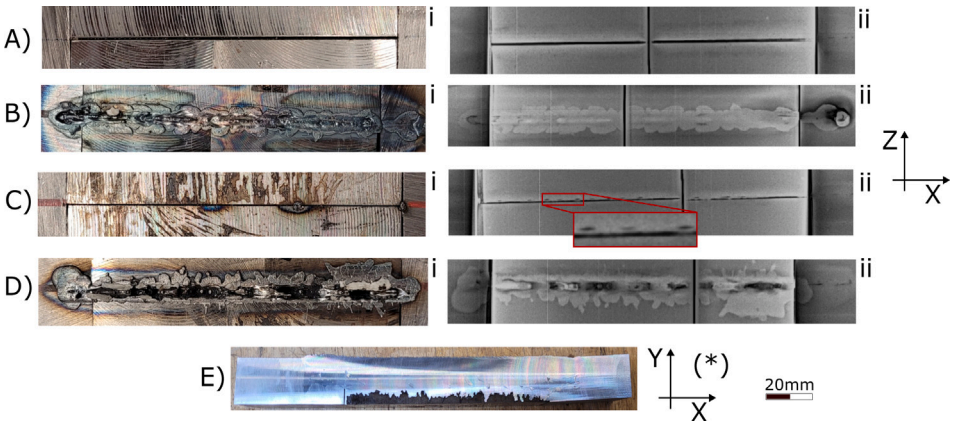

Fig. 7. Bottom, cut and X-ray figures, XZ plane. (*) XY plane.

enough molten material, these regions remain as cracks in the weld bead. This phenomenon occurs mainly in the separated sections within the weld bead.

In addition to X-ray inspection, samples P-CW6 (cut-wire), ML1 (only laser) and MM6 (double side) were also studied by EDX analysis, which showed no difference in the element distribution between them, although, for example, Zhang et al. [26] does find differences. These differences are very small and affect the Mn content. After several tests in the first welding stage, the steel backing sheet was decided to be used in some tests, instead of ceramic backing, since some samples showed root cavities due to the interaction of the laser beam with this backing, thus destroying the bottom of the joint. This was verified with a small series of tests. It was tested with 5 water cut samples that varied the power output. From the first to the third test, the power output was increased, obtaining in these 3 tests a lack of penetration, a small increase in the power output caused sample 4 to present root cavities, see Fig. 7(D). In the last test, the first power output configuration was repeated and root cavities occurred again. This may indicate that the line between the occurrence of lack of penetration or root cavities is very thin. This is the reason why the laser power was not always increased to the maximum, since higher values would not prevent root cavities. Other authors such as Wahbah et al. [11] showed the same behavior with the ceramic backing, according to them: “no matter how we changed the laser power or the welding speed, the same results are obtained; either partial penetration joint or full penetration joint with root cavities and underfill”.

According to Cheolhee et al. [27], in the case of copper backing, the back of the weld beads exhibited characteristics superior to those resulting from the use of ceramic backing. Thanks to the high thermal conductivity value of copper, it can help in solidification, according to Silva et al. [14]. In any case, the results regarding the use of steel backing are inconclusive, so more experiments about backing will be necessary for future research.

3.2.2. Macrograph

The laser-MAG hybrid welded joint consists of different parts: BM (base material), HAZ (heated affected zone) and WZ (weld metal zone) due to experiencing different thermal cycles during the welding process. Further, a special feature of this type of welding is the typical wine-cup shape that represents the transition between arc (top) and laser part (bottom).

Fig. 8 shows macrographs from the second stage of welding, each one corresponds to a different type of edge joint preparation. It is easy to observe the clear lack of penetration in the samples except for the case of the sample that had CW in its interior, no cracks or pores have been obtained in the macrographs. All samples show good quality at the top of the weld bead, although the MM sample has the highest penetration and some undercut defects. Although no macrographs of the first stage are shown, it is commented that the results in this aspect were similar, lack of penetration and no pores or cracks.

3.2.3. Microstructure

Regarding the microstructure results, no differences were found for the different types of edge joint preparation. The differences found in the microstructure are related to the power output applied to the sample. Those with the lowest applied power at the root of the weld bead show unfavorable microstructures due to the faster cooling. As there is no difference in the type of preparation, Fig. 9 shows the macrograph of a sample type ML, which is selected because it has full penetration. In addition, the figure shows the detailed microstructure of the various parts of interest in the sample. This sample belongs to the first welding stage. Fig. 9 of the ML8 sample shows the change in microstructure from the base material to the weld metal zone. The base material microstructure consists of a band structure of ferrite and pearlite phases and the direction of rolling can be seen in Fig. 9(a).

From the base material zone to the fusion zone, the following transition takes place: First, the pearlite spheroidizes and enters the

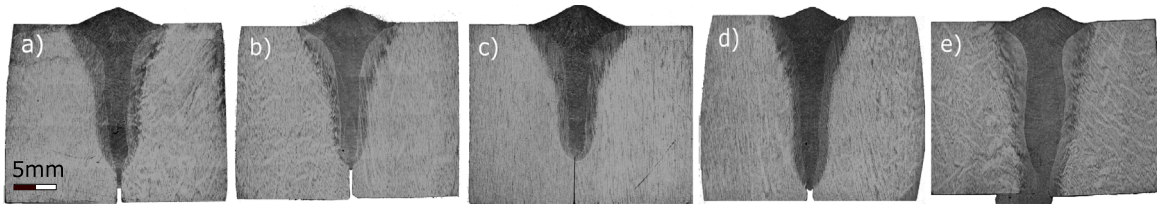

Fig. 8. Macrographs representing each of the sample edge joint preparation: (a) ML, (b) MH, (c) W, (d) MM and (e) P-CW.

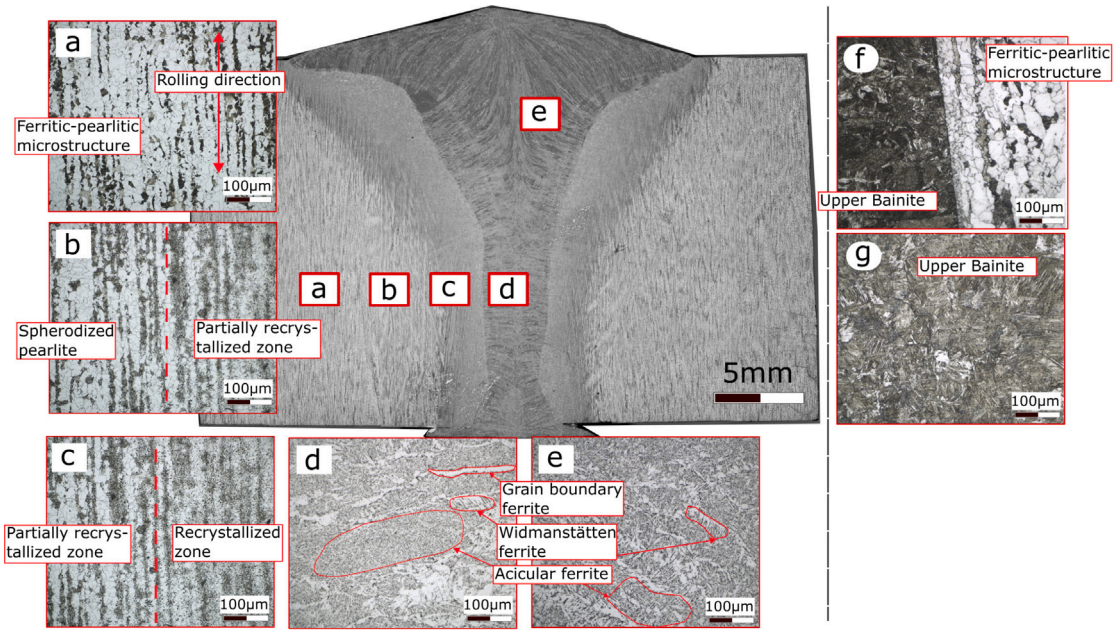

Fig. 9. Microstructure: Base material (a), partially recristalized zone (b), recristalized zone (c), laser fusion zone (d) and arc fusion zone (e) from ML8 sample. Lack of fusion (f) and overheated zone (g).

partially recrystallized zone (b). In the following image, the transition from the partially recrystallized zone to the recrystallized zone is shown (c). In the last images are shown the fusion zone, the arc dominated zone (e) and the laser dominated zone (d), where acicular ferrite, Windmannstatten ferrite and grain boundary ferrite can be seen. Generally, the laser dominated zone exhibited finer microstructure than the arc dominated zone, this is due to lower power output and thereby faster cooling rate, entails the laser zone being harder than the arc zone. As mentioned above, most of the samples showed a lack of penetration, this effect has a direct consequence on the formation of the microstructure and can be seen in Fig. 9(f). The lack of penetration can be seen as a lack of fusion at the joint edge, since it can be seen that there is no transition between the FZ and the BM. In addition, the effect generated in the microstructure when the power output is low, which results in very fast cooling rates and therefore an OHZ with an unfavorable microstructure (Fig. 9(g)), can also be appreciated.

The hybrid weld had the typical characteristic of an epitaxial solidification, and the columnar crystal grew perpendicular to the corresponding molten pool boundary. The growing columnar crystals within the laser zone were almost perpendicular to the weld center line, this being one of the most vulnerable weld regions [5]. According to Bunaziv et al. [21], reducing the cooling rates in the root by applying higher power output results in the formation of softer and more ductile microstructures. However, this can have a negative impact on mechanical properties as an undesirable microstructure may lead to a significant decrease in strength. In particular, the occurrence of coarse grains in the heat-affected zone (HAZ) often results in a notable reduction in toughness. However, fast cooling rates during welding can lead to the formation of brittle phases such as upper bainite. In multi-pass welding, this phenomenon is likely to happen frequently as subsequent passes preheat the HAZ areas. Zhen et al. [5] said that: "the Windmannstatten structure distributing the overheated zone might be one of the most important reasons making the welded joint embrittling". Authors such as Kannan et al. [7] showed in more detail the microstructures and the mechanical properties obtained for thick naval grade high strength low alloy steel in LAHW welding. Zhen et al. [5] also showed in more detail the microstructures and the mechanical properties for an S355J2W+N steel.

3.2.4. Tensile strength

Table 3 shows the tensile strength values of the different samples tested. According to the quality certificate of the supplier of the steel used for the tests, the yield strength is 353 MPa and the tensile strength measured is 549 MPa. All samples are close to this value. It is commented that some samples in the laser zone, due to the lack of penetration and lack of fusion in their walls, broke abruptly by the weld, this being an invalid result, that is why the letter 'X' is used in Table 3 to refer to these samples. The breakage zone of the remaining samples is always located in the base material.

According to Zhou et al. [23], a higher power output (within a certain range) can improve the tensile properties of the welded joints, although when the power output is too large, the tensile properties of the welded joints are reduced. Therefore, samples with higher power output (ML8, ML3 and MM6) have a lower elongation at break even though they break outside the weld zone as well.

3.2.5. Microhardness profile

Selected hardness data from the experiments showing the results for a comparison are shown in Figs. 10 and 11. Fig. 10(a) compared

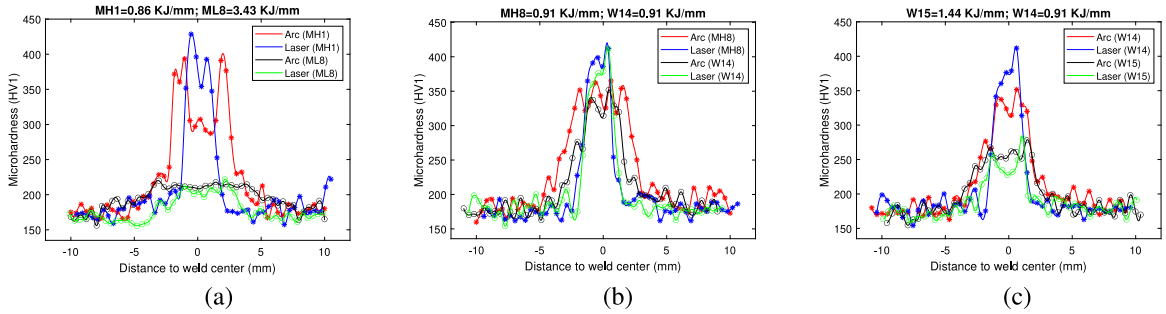

Fig. 10. Microhardness comparisons from the first set-up of welding: Maximum difference in power output and different surfaces (a), same power output and different surfaces (b) and different power output and same surfaces (c).

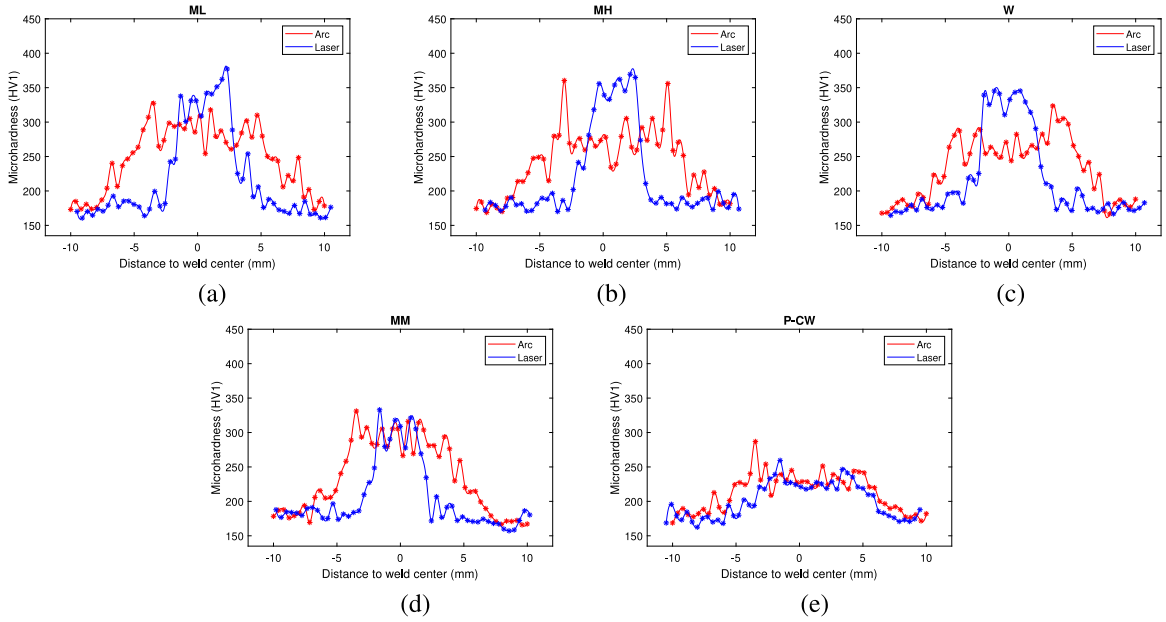

Fig. 11. Microhardness results from the second set-up of welding. (a), (b), (c), (d) power output 1.36 kJ/mm and (e) power output 1.92 kJ/mm.

the lowest power output with the highest. It was clear that when the power output was higher, the microhardness values were lower. Fig. 10(b) shows another comparison, it compares two samples with the same power output, but with a different joint preparation. The results are almost identical in values and behavior. Finally, within the same type of joint preparation, Fig. 10(c) shows that two different power outputs significantly affect the microhardness result. However, to a lesser extent than in case (a), because the difference between the two power output values is not that large. These results are in line with the findings of other authors such as Zhou et al. [23], they showed that the microhardness of welded joints of Q235 steel has relationship with the power output. The response obtained in terms of the microhardness profile is what was expected, since it can be seen that the hardness generally increases with decreasing line energy, according to Sørensen et al. [28]. High-line energies lead to more significant preheating, leading to lower cooling rates and ultimately lower hardness.

Fig. 11 shows the microhardness profile results from the second welding stage. (a) for the ML sample, (b) for the MH sample, (c) for the W sample, (d) for the MM sample, and (e) for P-CW sample. The following results can be extracted: Fig. 11(d) shows the MM sample, it had a greater penetration due to the fact that it had a larger gap volume than the other samples and therefore the melt could flow better towards the inside of the joint. In addition, the presence of an undercut could be appreciated in the upper part of the bead and in the laser zone, having lower microhardness values than the rest of the samples. Furthermore, due to a higher presence of the filler material from the arc torch in this zone of the weld bead. The rest of the samples (MH, ML and W) have completely similar behaviors among them. In all samples, the hardest point is on the laser part and in the fusion zone or the arc zone in the HAZ. In the present work, the highest hardness value was 428.6 HV1, which is the one with the smallest line energy applied. In Fig. 11(e) the microhardness profile of sample P-CW5 filled with cut-wire is shown. It was welded with 14 kW laser power and 600 mm/min of welding speed, obtaining 1.92 kJ/mm. In addition, the cut wire inserted into the joint was positioned so that it overflowed from the top. This increase in power output with respect to the rest of the samples in the second welding stage explains the drop in microhardness. It can also be seen that the curve representing the laser zone and the arc zone are similar, this is due to the presence of cut-wire in the laser zone, which means that these two zones do not differ in terms of hardness.

3.2.6. Impact toughness

In Table 3 can be seen the results of the Charpy test. No trend has been found in the results according to the different types of edge joint preparation. All samples showed ductile fracture, except samples ML8 and W19 (lower impact toughness values). In these samples, a larger cleavage zone was observed, characteristic of brittle fracture. Fig. 12 shows the cleavage zone of sample ML8 and its topographic surface that was obtained with the microscope. As can be seen in the rest of the image, most of the samples have a completely different type of breakage, ductile-type. If the toughness results are compared with the power output used in the sample, a slight increasing trend in toughness can

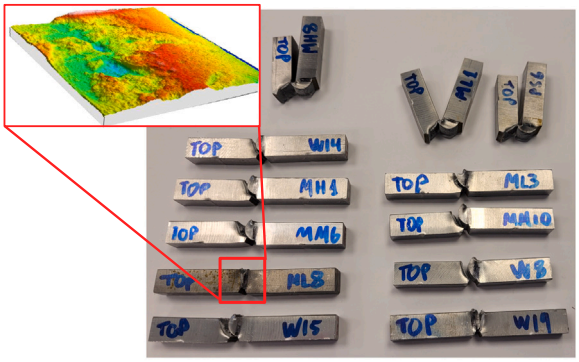

Fig. 12. Charpy test samples after testing. Note: The detail shows a topographic view from ML8 breakage zone.

be seen as the power output increases, discarding from the comparison those samples that have a brittle fracture. Bunaziv et al. [13] discussed that as the heat input in the sample increases, higher toughness values were achieved. They remarked that "this observation is possibly linked to softer microstructures that develop during slower cooling rates". They even mentioned that excessively high heat input (>2.0 kJ/mm) in the sample is proven to be detrimental for HAZ toughness. Also, they concluded that the lowest values were always associated with crack propagation along the FL, this trend could explain what happens with samples ML8 and W19.

Zhen et al. [5] worked with S355J2W + N and showed their results for the Charpy test performed at −40 °C, −20 °C and 20 °C. In addition, they did the notch in the WZ and obtained around 210 J. This value is of the same order as those obtained in this research (119.7 J–175.2 J). The difference is that they performed the notch in the WZ and not in the FL. Wang et al. [6] showed very interesting results, since they obtained Charpy impact values at −80 °C, −60 °C, −40 °C, −20 °C and 0 °C, (thus being able to show the ductile–brittle transition) for SAW versus LAHW specimens, performing the notch both in the molten metal zone, at the melt line and in the thermally affected zone. They selected an offshore engineering steel with a yield strength of 690 MPa. The result was that for both the FL and HAZ samples, the LAHW welded samples transitioned earlier from brittle to ductile.

3.3. Edge joint roughness impact on penetration depth in LAHW

Section 3.1 has shown how the quality of the surfaces was related to roughness measurement and Section 3.2.1 how the penetration values for each weld were obtained by machining the bottom of the weld bead. Fig. 13(a) shows the relationship between these two parameters, weld bead penetration obtained and roughness of the surface. To plot this, on the horizontal axis are placed the values ordered from lowest to highest roughness R_c(μm) of the surfaces studied in their 'Y' direction. Being the final order: ML, MH, W and MM. The vertical axis of the graph shows the penetration depth obtained. Gap and air volume gap are essential variables in obtaining higher penetration values. According to Polonsky et al. [29], the prescribed gap between the plates has a large impact on the tensile response of weldments. Nilsen et al. [30] showed that variations in joint gap width can produce imperfections in butt joint weld beads. The penetration results obtained according to these two variables are also shown. Fig. 13(b) shows the relationship between gap and penetration and Fig. 13(c) shows the relationship between air volume gap and penetration. In the case of Fig. 13(b) it can be seen how an increase in the gap produces an increase in penetration, in the same way that for Fig. 13(c), an increase in the air volume gap means an increase in penetration. For smaller gap size the penetration depth is consequently expected to be less, but for the water jet cut samples (having higher edge roughness) it is maintained, thereby showing a strong correlation with the increased surface roughness. For ML, MH, W and MM surfaces, 6 specimens have been made in order to check the repeatability, in the case of P-CW, 2 specimens have been made. P-CW samples are included in the graph but they are separated with a black line as they do not have the same welding parameters and it is also difficult to classify this type of joint by roughness as the cut-wire fill the joint. Furthermore, in the case of the air volume gap, it can only be welded by having the cut-wire added. It can also be seen that for all three cases, an increase in roughness, gap and air volume gap, an increasing trend in penetration is obtained. Authors such as Sokolov et al. [31] showed how the penetration of high power fiber laser welds with different roughness and gaps increased. They concluded that optimal welding results were obtained with high roughness values and gaps between 0.1 and 0.2 mm instead of 0 mm. This could be of great interest to industry, as they could consider welding the parts with a more rough preparation of the bevel or with larger gap tolerances. This would not only save pre-welding preparation time but also increase the penetration depth per pass.

It is therefore suggested by the authors that the result in penetration is due to the combined action of three effects, one at the micro scale and two at the macro scale. On the micro scale it would be the surface roughness and on the macro scale it would be both the gap used in the joint and the geometry of the profile (air volume gap). Authors such as Sokolov et al. [8] found a strong correlation between penetration depth and laser energy absorption due to surface roughness in the field of laser welding. Then, the energy efficiency of laser beam welding may be increased by edge preparation of the surface roughness. In addition, they found that the influence of the edge surface roughness on the penetration depth increases with the laser power level. In this work, they propose a possible explanation: Hagen-Rubens absorption relation for the wave-length of the fiber lasers used in the research. According to Sohail et al. [32], in keyhole mode laser welding, the amount of laser energy absorption greatly increases due to multiple reflections inside the keyhole and according to Obeidi et al. [33], the objective of their study was to study how surface roughness affects the dimensions of the meltpool and, consequently, the energy absorption during laser processing of stainless steel and aluminum. The impact of surface roughness is attributed to the occurrence of multiple reflections caused by increased surface irregularities, resulting in enhanced absorption of the incident radiation. The researchers conducted experiments using different roughness levels while keeping the laser parameters constant. They carefully analyzed the meltpool dimensions and observed that greater surface roughness correlated with significantly larger meltpools, indicating a corresponding increase in laser absorption.

At the macro scale, the MH, ML and W profiles are straight profiles, the difference between them is that the W profile has a gap of 0.3 mm, while the ML and MH profiles have a gap of 0.5 mm. This results in a different air volume in the joint in the case of water jet cut samples being 40% lower, making it more difficult for the molten metal to flow down into the weld bead. On a macro scale, the MM profile has a characteristic wave shape, which gives it an air volume in the joint 70% higher than the other machined surfaces ML and MH, which have the same 0.5 mm gap. For this reason, the MM samples show a more noticeable difference in the final result than the other samples (excluding cut-wire samples). According to Reithmeier et al. [34], they varied the gap between 0 and 0.5 mm and found that plates with 16 mm thick plates with gaps up to 0.3 mm could be bridged without changing the welding parameters. They concluded that with growing gap width, root humping can appear and undercut formation increases. In the case of plasma samples, the air in the joint is about 200% higher than the machined samples, so as mentioned above it is not possible to weld them with LAHW and it was decided to use the cut wire.

The welding process is initiated from the laser source, where all the beam energy is unleashed towards the process. During the transmission of the laser beam, a small percentage of around 1%–5% energy may be lost due to scattering and reflection in the optics and focusing systems.

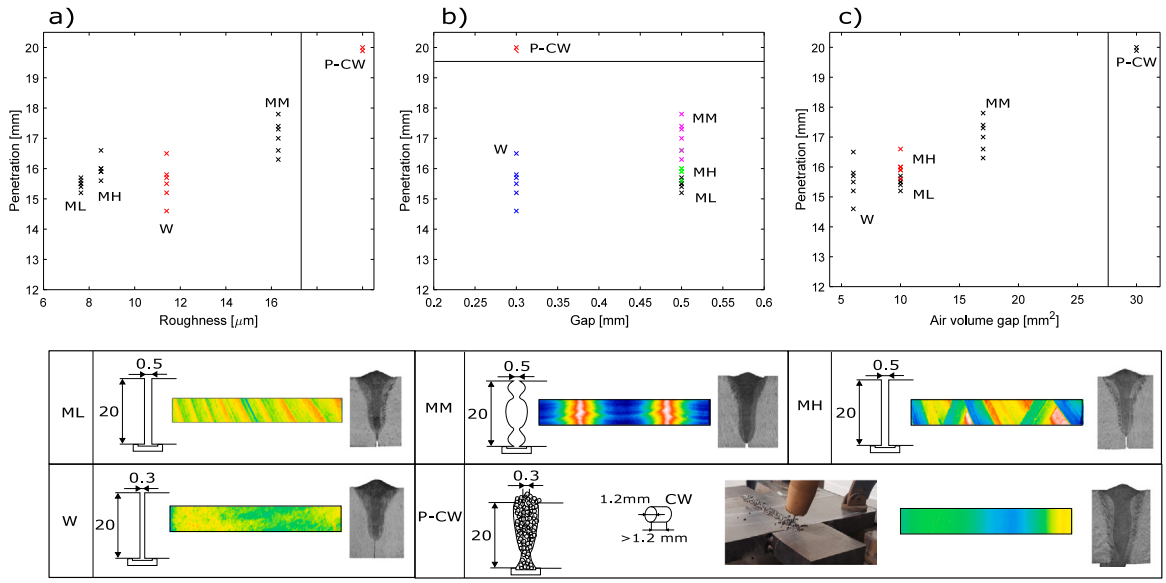

Fig. 13. Edge joint preparation impact on penetration depth in LAHW.

Before the laser beam is caught by the melt pool then fumes in and around the keyhole absorbs a fraction of the energy. Berczeli et al. [35] shows that roughly 90% of the laser beam energy is absorbed in the keyhole. When the laser beam enters the keyhole multiple reflections on the walls gradually absorbs the beam energy. The laser beam energy is caught by the surface of the material where a certain degree of the laser beam is absorbed, and the rest, approximately around 5%–10%, is reflected. The ratio is very dependent on factors as temperature and incident angle. The remaining beam energy that is absorbed by the material and used to melt and generate the weld bond. This amount sums up to be between 70%–80% of the initial laser energy. Within the molten material, a small part of the absorbed laser energy is dissipated through thermal conduction and other losses, which could be around 5%. Finally, the remaining energy around 10%–15% is distributed towards the joint walls. Due to the low percentage of energy from the laser that is actually in contact with the walls of the weld joint, there may be another explanation for why greater penetration is obtained when the roughness is increased. This explanation could lie in the behavior of the molten metal. In addition, according to Powell et al. [36], inside the keyhole, melt flow is pushed downward by the evaporation force of the laser and by the action of gravity. Although, "the mass flow around the keyhole in the direction of welding must be approximately equal the weld cross section multiplied by the welding speed multiplied by the material density". So clearly, there is molten material in front of the laser beam in the welding direction. Powell et al. [36] showed this from finite element simulations. Some recent research showed the molten pool behavior during laser beam welding, where actually a melt film is surrounding the keyhole, also at the keyhole front. Therefore, the laser beam actually do not hit the edges. Yang et al. [37] studied the effect of the oscillating metal vapor plume on the keyhole and molten pool behavior by numerical methods, and they validated their results through experiments. Meng et al. [38] showed the influence of the spatial laser energy absorption on the molten pool dynamics with numerical simulations. Bachmann et al. [39] evaluated the mechanisms of the evolution of a narrowed region in the weld pool center, also supported by validation of experimental results. Meng et al. [40] proposed a model that provides accurate predictions to the variation of penetration depth and weld pool profiles caused by the magnetohydrodynamics effect. In this case, the authors validated the results by the measurements of optical micrographs and in-situ metal/glass observation. Reinheimer et al. [41] concluded that the elongation of the keyhole is a consequence of a supercritical stream of the melt flowing underneath and around the keyhole. X-ray images of the keyhole and cross-sections of the weld were used in their research. Bakir et al. [42] worked on the influence of weld pool geometry on solidification cracking in partial penetration welds using thick steel plates.

Fig. 14 shows the proposed evolution of the molten pool for the welds in this research. Cross-section A-A′ shows the formation of the keyhole and the melt pool and how this molten metal interacts first with the roughness of the joint edges. This has been expanded in detail B* from cut B-B′, where it is possible to see how the molten metal interacts with the roughness of the walls. The concern is therefore the behavior of the molten material inside the joint. The phenomenon of thermocapillarity is present as the molten pool would tend to flow into areas of lower resistance. This can cause the molten material to be distributed along the joint between the walls, filling the spaces between them. Thus, if the walls have a higher roughness, they may have surface irregularities. These irregularities can influence the way the molten pool flows along the joint. In some cases, a rougher surface can create more space for the molten material to spread out, facilitating penetration and bonding between the walls. Authors such as Heider et al. [43] studied keyhole instabilities during welding with high-speed X-ray imaging. They showed that bubble formation at the tip of the capillary is one mechanism which causes weld defects like pores. This method is a very effective way of finding out what is going on inside the joint.

Regarding the behavior of the cut-wire samples (Fig. 15), it could be that the melt pool at the front of the laser beam is larger than in the case of samples that do not have cut-wire. The power output is higher for these samples than for those without the cut-wire in the joint, so that it can melt all the cut-wire elements. Thanks to the increased molten pool and the pressure of the keyhole vapor pushing the molten metal downwards it is able to achieve full penetration. Notice the difference in the width of the weld bead between the macrograph section (Fig. 8(e)) with the cut-wire and the rest of the sections without the cut-wire. In this case, the effect of the roughness of the walls would be completely overshadowed by the addition of the cut-wire.

According to Xiao et al. [44], in the liquid melt pool during laser welding, there are four forces acting on the fluid flow: buoyancy force, originate from the spatial variation of the liquid-metal density; Marangoni force, originate from surface tension gradients; gravity and shear force, originate from laser induced vapor or plasma. In this case, LAHW is performed, so it is necessary to take into account the

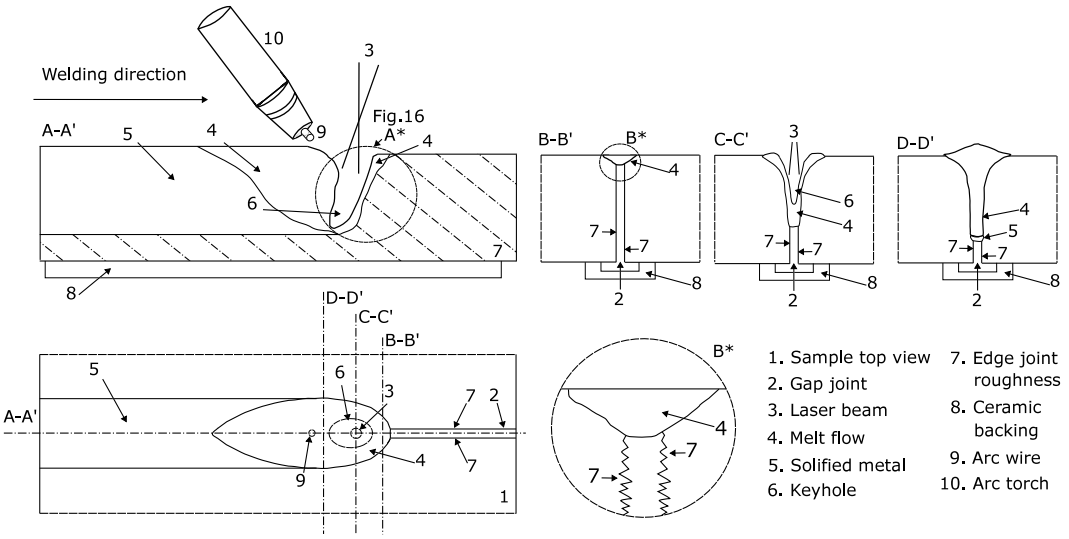

Fig. 14. Evolution of the molten pool in LAHW welding. (Note: Non-scale drawing.)

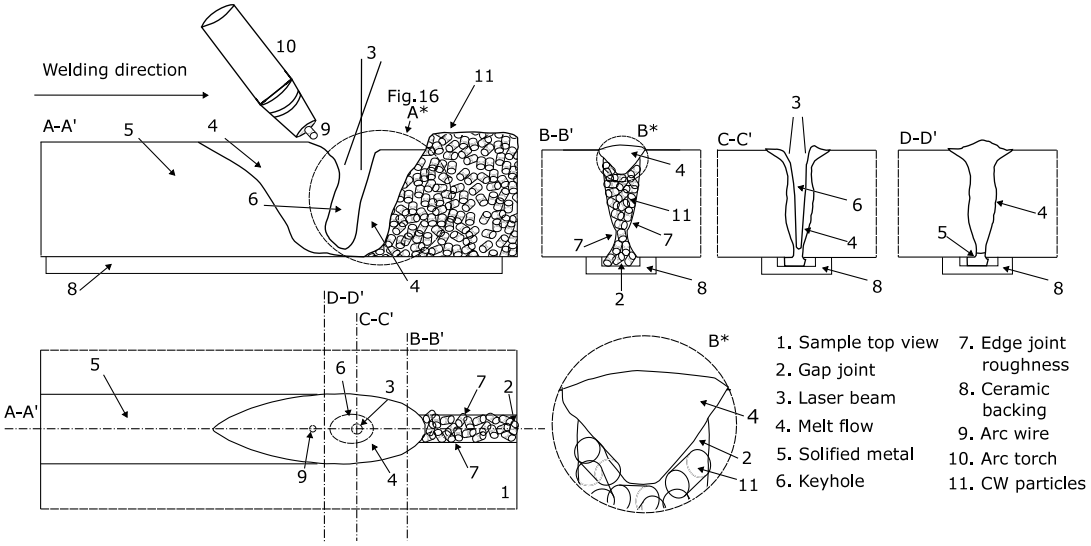

Fig. 15. Evolution of the molten pool in LAHW welding with cut-wire samples. (Note: Non-scale drawing.)

effect of using the arc torch. This would be taken into account by adding the Lorentz force, since the electric current in the workpiece converges towards the electrode and hence near the center of the pool surface [45]. The flow in melt pool is mainly derived by spatial variation of the surface tension, which is known as thermocapillary flow or Marangoni convection [44]. Other authors such as Artinov et al. [46] showed the physics behind the keyhole mode welding process includes some physical aspects such as keyhole formation, thermocapillary and natural convection of the liquid metal, heat conduction in the weld pool and in the solid part and surface heat transfer.

Fig. 16 shows the force diagrams for the samples without and with cut-wire, both at the bottom and at the top of the melt pool in front of the keyhole. The vapor pressure of the keyhole pushes the weld pool forward, downwards and around the keyhole. The arrows representing the keyhole vapor pressure (number 6) are drawn tilted downwards because they are the combined action of the vapor pressure and the vaporization of the melt. In addition, the pressure caused by the wetting is also drawn (number 7), which slows down the progress of the molten pool. The wetting capability depends on surface roughness condition, temperature gradient and material composition. Surface roughness conditions will provide different wetting conditions, so high surface roughness, will provide better wetting conditions and therefore better penetration. This would explain the result of samples with the same gap and different roughness, see Fig. 17. Furthermore, inside the melt pool, with more equal temperature gradient, better wetting capability. In samples without cut-wire inside, the gap is much smaller, so the pressure in the joint and consequently the surface tension will be higher than in the case of samples with cut-wire inside (the cut-wire pieces are stuck in the joint). The decrease in the surface tension in the cut-wire samples can make the melt pool in front of the keyhole larger as a result.

According to Frostevarg et al. [47], the melt experiences a gravitational pressure plus the pressure in the melt by the keyhole vapor. This is counteracted by the surface tension σ, acting upwards at the edges of the gap, having an equilibrium between downward (P_k) and upward forces (P_σ).

$$P_k = P_{keyhole} + P_{Gravity}$$

P_σ is the surface tension and F_σ is the wetting, that is force produced by surface tension acting along the solid–liquid interface. The magnitude of this force is angle dependent. Surface tension is characterized by

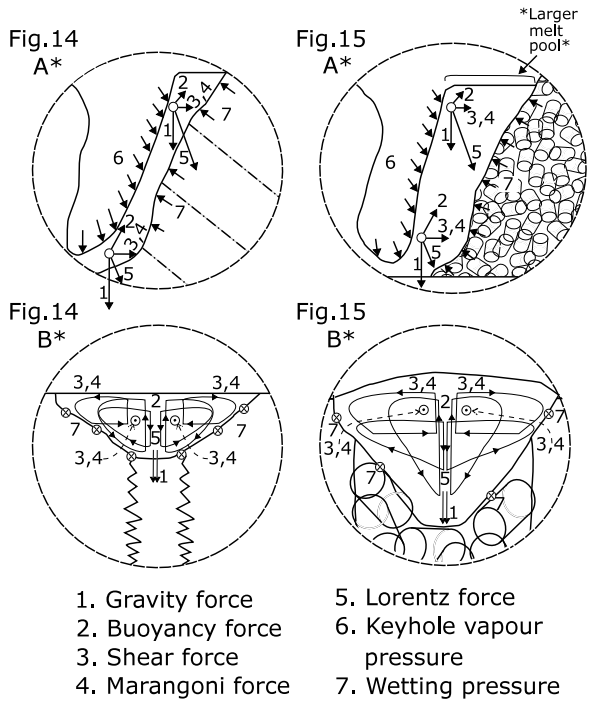

Fig. 16. Force diagram in detail sections A* and B* for LAHW welds without and with CW. (Note: Non-scale drawing.)

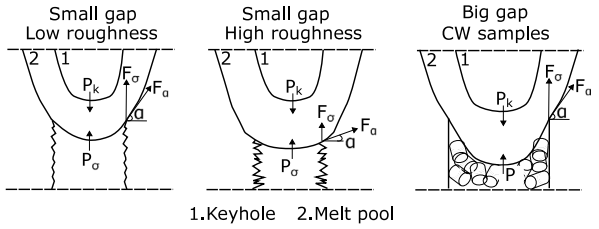

Fig. 17. Dimensional description for surface tensional forces for small/big gap and low/high roughness cases. (Note: Non-scale drawing.)

the liquid and wetting is characterized by the solid–liquid interaction.

$$F_\sigma = C \cdot \sigma \cdot sin(\alpha)$$

Comparing the three cases in Fig. 17, when F_σ is lower there is better wetting conditions and as a result better penetration of the molten pool. This can be seen by looking at the end of the weld bead in macrographs (a), (b) and (c) in Fig. 8.

This theoretical explanation is presented as a first approximation of what may be happening inside the joint when the roughness is varied. For future research, it would be considered high speed video system to study these phenomena in the cavity as in the research of Wiklund et al. [48], Kim et al. [49], Karlsson et al. [50] and Iliar et al. [51], where they studied welding with increasing gap, through high speed video. And also using X-ray imaging as in previously cited papers.

4. Conclusions

In this research, a study of the relationship between different edge preparation methods and the penetration obtained in the weld bead has been carried out. The tests were carried out on 20 mm thick S355J2 steel specimens welded using different combinations of LAHW welding parameters. The following conclusions have been drawn:

- An increasing trend of penetration with increasing sample roughness, gap and air volume gap has been observed. On the one hand, the wetting capability of the molten metal will increase, i.e. it will flow more easily through the joint when the edge joint is rougher. On the other hand, if the volume of air in the joint is larger, this will also allow the molten material to flow to the bottom of the joint more easily and thus ultimately achieve greater penetration. Furthermore, a theoretical explanation for this phenomenon has been proposed. Therefore, in an industrial environment where beveling is carried out, it would be recommended that the beveling be rougher.
- The cut-wire samples are at full penetration and without defects, even without the presence of undercuts considering the large air volume gap present inside their joint. With a slight increase in power output together with the cut-wire this full penetration is achieved. The melt pool in front of the keyhole is increased by the addition of the cut-wire and the vapor pressure of the keyhole pushes this extra molten metal downwards. One of the potential problems facing the plasma cut samples was that their large air volume gap was incapable of being welded with LAHW. Since the laser would be in contact only with the lower part of the joint where the burr produced by the plasma cut is located. Then the laser would destroy the bottom part of the joint contacting the ceramic backing because there is insufficient material and the laser would not be in contact with the top part of the joint due to the size of the gap. From what has been shown in this research, the cut-wire particles made welding possible even under these unfavorable conditions. The use of cut-wire is therefore of interest for industrial applications with non-beveled joints, or in joints that are beveled but have defects. For example, in bevel preparation there is accepted tolerances with gaps, this can be completely constraining for the laser. The use of cut-wire implemented in the joint can achieve welding even with a certain gap increase.
- The mechanical properties of the welds have been verified from tensile test, Charpy test and microhardness profiles. Proper tensile strength results for all specimens and proper failure of most Charpy specimens have been obtained. No relationship is found between the results of the mechanical properties and the different edge joint preparation. However, differences are found depending on the power output applied to the samples, since microhardness levels increases with decreasing applied line energy. Furthermore, it can be seen from the microhardness results that the presence of the electrode in the lower parts (laser zone) results in lower microhardness levels, either because a large gap has allowed the fluid to flow down the joint more easily or because cut-wire has been added. With the parameter settings used in the research, defects such as pores, cracks, or undercuts were rarely found, validated by X-ray and visual inspection. However, a lack of penetration has occurred in most of the samples.

CRediT authorship contribution statement

A. Artero-Real: Writing – review & editing, Writing – original draft, Visualization, Investigation, Formal analysis, Data curation, Conceptualization. **M. Kristiansen:** Writing – review & editing, Supervision, Resources, Project administration, Methodology, Conceptualization. **J. Frostevarg:** Writing – review & editing, Supervision, Methodology, Conceptualization. **J. Justo:** Writing – review & editing, Supervision, Project administration, Funding acquisition, Conceptualization. **J. Cañas:** Writing – review & editing, Supervision, Project administration, Funding acquisition, Conceptualization.

Declaration of competing interest

The authors declare that they have no known competing financial interests or personal relationships that could have appeared to influence the work reported in this paper.

Data availability

Data will be made available on request.

Declaration of Generative AI and AI-assisted technologies in the writing process

During the preparation of this work the author(s) used 'DeepL write' in order to improve some sentences in English. After using this tool/service, the author(s) reviewed and edited the content as needed and take(s) full responsibility for the content of the publication.

Acknowledgments

This research has been developed in the FLOATWIND project associated with the RESEARCH OF NEW TECHNOLOGICAL SOLUTIONS FOR DESIGN AND MANUFACTURING OF SUPERSTRUCTURES FOR FLOATANT MARINE WIND ENERGY with official code PNA-020100-2023-2 which is part of the PERTE NAVAL Strategic Project for the Recovery and Economic Transformation for the modernization and diversification of the Spanish naval ecosystem (PERTE NAVAL) of the Ministry of Industry and specifically of the approved project INNCODIS: DEVELOPMENT OF AN INNOVATIVE INDUSTRIAL ECOSYSTEM FOR A COMPETITIVE, DIVERSIFIED AND SUSTAINABLE NAVAL SECTOR led by Navantia. Furthermore, the authors of the University of Seville would like to thank Aalborg University for allowing the corresponding author to spend two stays there and to use their facilities. Thanks to Mikael Larsen from Department of Materials and Production, Aalborg University for helping in microstructure analysis.

References

[1] S. Webster, Y. Tkach, P. Langenberg, A. Nonn, P. Kucharcyzk, J. Kristensen, P. Courtade, L. Debin, Hyblas: economical and safe laser hybrid welding of structural steel, Eur. Comm. (2009).
[2] S. Nielsen, High power laser hybrid welding – challenges and perspectives, Physics Procedia 78 (2015).
[3] I. Bunaziv, X. Ren, V. Olden, A comparative study of laser-arc hybrid welding with arc welding for fabrication of offshore substructures, J. Phys. Conf. Ser. 2626 (2023).
[4] C. Churiaque, M. Chludzinski, M. Porrua-Lara, A. Dominguez-Abecia, F. Abad-Fraga, J.-M. Sánchez-Amaya, Laser hybrid butt welding of large thickness naval steel, Metals (2019).
[5] S. Zhen, Z. Duan, D. Sun, Y. Li, D. Gao, H. Li, Study on microstructures and mechanical properties of laser–arc hybrid welded S355J2W + N steel, Opt. Laser Technol. 59 (2014).
[6] X. Wang, W. Su, Z. Xie, X. Li, W. Zhou, C. Shang, Q. Wang, J. Bai, L. Wu, Microstructure evolution of heat-affected zone in submerged arc welding and laser hybrid welding of 690 MPa high strength steel and its relationship with Ductile–Brittle transition temperature, Acta Metall. Sin. (2022).
[7] M.V. Kannan, N. Arivazhagan, M.N. Rao, G.M. Reddy, K.P. Prabhakar, P. Gadhe, Studies on microstructure and mechanical properties of weldments produced in 12 mm thick naval grade high strength low alloy steel for sub-zero application by single and double pass hybrid laser arc welding, J. Mater. Eng. Perform. (2021).
[8] M. Sokolov, A. Salminen, V. Somonov, A.-F. Kaplan, Laser welding of structural steels: Influence of the edge roughness level, Opt. Laser Technol. 44 (2012).
[9] M. Sokolov, A. Salminen, The effect of joint edge surface preparation on the efficiency of fiber laser welding of low-alloyed steels, Mechanika 21 (2015) 220–225.
[10] F. Farrokhi, M. Kristiansen, A practical approach for increasing penetration in hybrid laser-arc welding of steel, Physics Procedia 83 (2016).
[11] M. Wahba, M. Mizutani, S. Katayama, Single pass hybrid laser-arc welding of 25 mm thick square groove butt joints, Mater. Desing 97 (2016).
[12] I. Bunaziv, O.-M. Akselsen, J. Frostevarg, A.-H. Kaplan, Laser-arc hybrid welding of thick HSLA steel, J. Mater. Process. Technol. 259 (2018).
[13] I. Bunaziv, C. Dørum, S.-E. Nielsen, P. Suikkanen, X. Ren, B. Nyhus, M. Eriksson, O.-M. Akselsen, Laser-arc hybrid welding of 12- and 15-mm thick structural steel, Int. J. Adv. Manuf. Technol. 107 (2020).
[14] R. Gomes, M. Baranenko, M. Pereira, K. Faes, Evaluation of high penetration hybrid laser-GMAW welding process productivity applied in the joining of thick plates, Int. J. Adv. Manuf. Technol. 121 (2022).
[15] T. Uemura, K. Gotoh, I. Uchino, Expansion of laser–arc hybrid welding to horizontal and vertical-up welding, Weld. World 66 (2022) 495–506.
[16] Ö. Üstündağ, A. Fritzsche, V. Avilov, A. Gumenyuk, M. Rethmeier, Hybrid laser-arc welding of thick-walled ferromagnetic steels with electromagnetic weld pool support, Weld. World 62 (2018).
[17] O. Üstündağ, A. Fritzsche, V. Avilov, A. Gumenyuk, M. Rethmeier, Study of gap and misalignment tolerances at hybrid laser arc welding of thick-walled steel with electromagnetic weld pool support system, Procedia CIRP 74 (2018).
[18] Ö. Üstündağ, N. Bakir, S. Gook, A. Gumenyuk, M. Rethmeier, Hybrid laser-arc welding of laser- and plasma-cut 20-mm-thick structural steels, Weld. World 66 (2022).
[19] F. Farrokhi, S. Nielsen, R. Schmidt, S. Pedersen, M. Kristiansen, Effect of cut quality on hybrid laser arc welding of thick sections steels, Physics Procedia 78 (2015).
[20] I. Bunaziv, J. Frostevarg, O.-M. Akselsen, A.-F. Kaplan, Hybrid welding of 45 mm high strength steel sections, Physics Procedia 89 (2017).
[21] I. Bunaziv, O.-M. Akselsen, J. Frostevarg, A.-H. Kaplan, Deep penetration fiber laser-arc hybrid welding of thick HSLA steel, J. Mater. Process. Technol. 256 (2018).
[22] I. Bunaziv, C. Dørum, S.-E. Nielsen, P. Suikkanen, X. Ren, B. Nyhus, M. Eriksson, O.-M. Akselsen, Root formation and metallurgical challenges in laser beam and laser-arc hybrid welding of thick structural steel, Int. J. Adv. Manuf. Technol. 116 (2021).
[23] S. Zhou, T. Yan, W. Muneer, X. Yin, Q. Gao, X. Zhan, Effect of heat input on LMHMW joint of carbon steel, Appl. Sci. 12 (301) (2022).
[24] F. Farrokhi, R.-M. Larsen, M. Kristiansen, Single pass hybrid laser welding of 25 mm thick steel, Physics Procedia 89 (2017).
[25] T. Hassel, R. Konya, M. Collmann, P. Schaumann, S. Priebe, T. Deißer, A. Beniyash, N. Murray, F.-W. Bach, Economical joining of tubular steel towers for wind turbines employing non-vacuum electron beam welding for high-strength steels in comparison with submerged arc welding. [international institute of welding], Weld. World 57 (2013) 551–559.
[26] C. Zhang, G. Li, M. Gao, X.-Y. Zeng, Microstructure and mechanical properties of narrow gap laser-arc HybridWelded 40 mm thick mild steel, Materials 10 (106) (2017).
[27] C. Kim, Back bead characteristics during butt welding of a thick plate for various backing conditions, Mater. Sci. Forum 654 (2011) 350–353.
[28] C. Sørensen, A. Nissen, C. Brynning, J. Nielsen, R. Schøn, R. Malefijt, M. Kristiansen, Double-sided hybrid laser-arc welding of 25 mm S690QL high strength steel, in: 18th Nordic Laser Materials Processing Conference, 18th NOLAMP, 2021.
[29] A. Polonsky, J. Madison, M. Arnhart, H. Jin, K. Karlson, A. Skulborstad, J. Foulk, S. Murawski, Toward accurate prediction of partial-penetration laser weld performance informed by three-dimensional characterization – Part I: High fidelity interrogation, Tomogr. Mater. Struct. 2 (2023).
[30] M. Nilsen, F. Sikstrom, A.-K. Christiansson, A. Ancona, Monitoring of variying joint gap width during laser beam welding by a dual vision and spectroscopic sensing system, Physics Procedia 89 (2023).
[31] M. Sokolov, A. Salminen, Experimental investigation of the influence of edge morphology in high power fiber laser welding, Physics Procedia 39 (2012) 33–42.
[32] M. Sohail, S.-W. Han, S.-J. Na, A. Gumenyuk, M. Reithmeier, Numerical investigation of energy input characteristics for high-power fiber laser welding at different positions, Int. J. Adv. Manuf. Technol. 80 (2015) 931–946.
[33] M.-A. Obeidi, E. McCarthy, S.-I. Ubani, U. Ahad, D. Brabazon, Effect of surface roughness on CO2 laser absorption by 316L stainless steel and aluminum, Mater. Perform. Charact. 8 (6) (2019).
[34] M. Rethmeier, S. Gook, M. Lammers, A. Gumenyuk, Laser-hybrid welding of thick plates up to 32 mm using a 20 kW fibre laser, Q. J. Japan Weld. Soc. 27 (2009).
[35] M. Berczeli, G. Buza, Relationship between the keyhole laser welding and the plasma, IOP Conf. Ser.: Mater. Sci. Eng. 448 (2018).
[36] J. Powell, T. Ilar, J. Frostevarg, M.-J. Torkamany, S.-J. Na, D. Petring, L. Zhang, A.-F.-H. Kaplan, Weld root instabilities in fiber laser welding, J. Laser Appl. 27 (2) (2015).
[37] F. Yang, X. Meng, S.-N. Putra, A. Artinov, M. Bachmann, M. Rethmeier, Numerical analysis of the effect of an oscillating metal vapor plume on the keyhole and molten pool behavior during deep penetration laser beam welding, J. Laser Appl. 35 (2023).
[38] X. Meng, S.-N. Putra, M. Bachmann, M. Rethmeier, Influence of the spatial laser energy absorption on the molten pool dynamics in high-power laser beam welding, J. Laser Appl. 35 (2023).
[39] M. Bachmann, X. Meng, A. Artinov, M. Rethmeier, Evaluation of narrowed weld pool shapes and their effect on resulting potential defects during deep penetration laser beam welding, J. Laser Appl. 34 (2022).
[40] X. Meng, M. Bachmann, A. Artinov, M. Rethmeier, A study of the magneto-hydrodynamic effect on keyhole dynamics and defect mitigation in laser beam welding, J. Mater. Process. Technol. 307 (2022).
[41] E.-N. Reinheimer, P. Berger, C. Hagenlocher, R. Weber, T. Graf, Supercritical melt flow in high-speed laser welding and its interdependence with the geometry of the keyhole and the melt pool, Int. J. Adv. Manuf. Technol. (2024).
[42] N. Bakir, O. Üstündağ, A. Gumenyuk, M. Rethmeier, Influence of the weld pool geometry on solidification cracking in partial penetration high power laser beam welding, Procedia CIRP 111 (2022).

[43] A. Heider, J. Sollinger, F. Abt, M. Boley, R. Weber, T. Graf, High-speed X-Ray analysis of spatter formation in laser welding of copper, Physics Procedia 41 (2013) 112–118.
[44] X. Xiao, C. Lu, Y. Fu, X. Ye, L. Song, Progress on experimental study of melt pool flow dynamics in laser material processing, Liquid Metals (2020).
[45] S. Kou, Welding Metallurgy, John Wiley & Sons, Inc., 2003.
[46] A. Artinov, V. Karkhin, P. Khomich, M. Bachmann, M. Rethmeier, Assessment of thermal cycles by combining thermo-fluid dynamics and heat conduction in keyhole mode welding processes, Int. J. Therm. Sci. 145 (2019).
[47] J. Frostevarg, Factors affecting weld root morphology in laser keyhole welding, Opt. Lasers Eng. 101 (2018) 89–98.
[48] G. Wiklund, O. Akselsen, A. Sørgjerd, A. Kaplan, Geometrical aspects of hot cracks in laser-arc hybrid welding, J. Laser Appl. 26 (2014).
[49] Y. Kim, N. Alam, H. Bang, H. Bang, Observation of hybrid (cw Nd:YAG laser + MIG) welding phenomenon in AA 5083 butt joints with different gap condition, Sci. Technol. Weld. Join. 11 (2006) 295–307.
[50] J. Karlsson, P. Norman, A. Kaplan, P. Rubin, J. Lamas, A. Yañez, Observation of the mechanisms causing two kinds of undercut during laser hybrid arc welding, Appl. Surf. Sci. 257 (2011) 7501–7506.
[51] T. Ilar, I. Eriksson, A. Kaplan, Simultaneous top and root high speed imaging on droplet formation in laser welding, in: 32nd Int. Congr. Appl. Lasers Electro-Optics, 2013.